

Nonlinearity Compensation Based on Identified NARX Polynomials Models

Lucas A. Tavares, Petrus E. O. G. B. Abreu and Luis A. Aguirre

Abstract—This paper deals with the compensation of nonlinearities in dynamical systems using nonlinear polynomial autoregressive models with exogenous inputs (NARX). The compensation approach is formulated for static and dynamical contexts, as well as its adaptation to hysteretic systems. In all of these scenarios, identified NARX models are used. The core idea is to rewrite the model as an algebraic polynomial whose roots are potential compensation inputs. A procedure is put forward to choose the most adequate root, in cases where more than one is possible. Both numerical and experimental results are presented to illustrate the method. In the experimental case the method is compared to other approaches. The results show that the proposed methodology can provide compensation input signals that practically linearize the studied systems using simple and representative models with no more than five terms.

Note to Practitioners—Nonlinearities impose significant performance limitations over a wide range of industrial applications, such as actuators and sensors. In many cases, classical control methods can present distress to deal with these effects. This paper is motivated by the use of compensation methods to improve the efficiency and quality of closed loop applications. Our goal is to present a practical technique based on NARX models for designing compensators. The method is tested with numerical examples, such as a model that describes a heating system with polynomial nonlinearity, and a hysteretic model to describe a piezoelectric actuator. An experimental pneumatic valve that presents several types of nonlinearities, including hysteresis or dead-zone, is used to illustrate the performance on a practical system. As we propose a general method, the approach is also applicable to other systems modeled by NARX models.

Index Terms—Compensation of nonlinearities, static and dynamic compensation, hysteresis compensation, NARX polynomials, pneumatic valve.

I. INTRODUCTION

NONLINEAR system identification is now a mature field. For the last three decades, much attention has been paid to the problem of building nonlinear models from data [1]–[4]. A natural next step is the use of such identified models in more specific applications, such as compensation and control, which is the aim of this work.

The presence of nonlinear effects can impose significant performance limitations in a wide range of applications, such as actuators [5], [6], sensors [7], pH neutralization [8], and power systems [9], among others [10]–[12]. A natural solution would be to mitigate such effects by making the systems more

linear – by using a compensator – and, consequently, more amenable to control. A dynamical model with simple structure is quite useful to design a compensator.

Compensation approaches aim to design a compensation input that reduces nonlinearity allowing for more accurate control and tracking. Many of these approaches start with an appropriate model that represents the most fundamental aspects of the system, especially the static nonlinearity [13]. In the literature, there is a vast number of works devoted to the modeling and compensation for nonlinear systems ranging from those based on phenomenological models [5], [14], [15] to those that use computational intelligence [16] such as Radial Basis Functions (RBFs) [6], [7], [17] and Neural Networks (NNs) [9], [18]–[20], among others.

The identification of phenomenological models tends to be a challenging task that requires sophisticated algorithms based often on heuristics techniques. Therefore, satisfactory results depend largely on the proper design of these algorithms, including the tuning of meta-parameters, which is usually an empiric task [16]. In addition, the achievement of compensators for such models is not usually simple or even possible, because it depends on the analytical inversion of these models. For methods based on universal approximation of functions, such as RBFs and NNs, it is more difficult to provide a physics-based interpretation [16]. A particular type of neural network that has been often used in the literature for identification and compensation of nonlinear systems is the Nonlinear AutoRegressive with eXogenous inputs Neural Networks, i.e., NARX NNs [18], [20]. Despite the benefits of NARX NNs due to the fair generality presented by NARX structures, these frameworks are based on a black-box philosophy that complicates the use of constraints related to the structure or parameters, which can be elegantly accommodated in gray-box approaches [21]. Also, their compensators present low or no degree of interpretability which limits the analysis of these types of models and their compensators.

An alternative framework is based on NARX polynomial models, adopted in this paper. For this class of models, if the structure is carefully chosen [22]–[24], besides being quite general [25], such models can encode nonlinear information in a simple and recognizable way [13], [26], which allows using them to derive explicitly compensation laws [21]. In addition, NARX polynomials are amenable to gray-box techniques [27] that allow the encoding relevant features from nonlinear systems, which is usually not possible with purely black-box strategies. From now on, the term NARX models must be understood strictly as NARX polynomial models, and form the basis of this work. Although these models can represent

Manuscript received November 24, 2020.

L. A. Tavares and P. E. O. G. B. Abreu are with the Graduate Program in Electrical Engineering, Universidade Federal de Minas Gerais, Belo Horizonte, MG, Brazil (e-mails: amarallucas@ufmg.br; petrusabreu@ufmg.br).

L. A. Aguirre is with the Department of Electronic Engineering, Universidade Federal de Minas Gerais, Belo Horizonte, MG, Brazil (e-mail: aguirre@ufmg.br).

a variety of phenomena, few works in the literature apply NARX polynomials for compensation since the most common applications take NARX NNs as a basis.

In the context of hysteresis compensation, [28] has presented a strategy based on an analytical inversion of NARX models. For this purpose, somewhat restrictive assumptions must be satisfied by the model structure. Also, as pointed out in [21], the methodology developed by [28] may suffer from singularity problems when the velocity variable equals zero.

Two ways to design compensators have been presented in [21]: the first one is similar to what was done in [28] and the second seeks compensators directly from the data. Both strategies have overcome the singularity problem because the restrictions on the models' structure prevent a division by the velocity variable in the compensator. However, as the former also needs to isolate the input explicitly, such a method uses with more specific structures than those used in the present paper. The second strategy requires careful data processing, such as filtering the output signals. Also, some algebraic tricks are required to overcome potential causality problems [21].

The main contributions of this work are the proposed approaches to find compensation inputs iteratively for nonlinear systems in static and dynamical contexts through identified NARX models. Besides, an adaptation of the dynamical strategy is presented for hysteretic systems. In both strategies, an algebraic polynomial of the compensation input is formulated, which is achieved by manipulating the identified model. Thus, the compensation input signal is calculated iteratively, which confers an adaptive feature to the approaches. The proposed compensators are compared with one well-established [5] and two recent [21] ones. The comparison is not performed with [28] due to the similarity with the first method of [21].

This work is organized as follows. In Section II background is provided. The statement of the compensation problem is introduced in Sec. III. Section IV presents the compensation strategy proposed and formulated for static (IV-A), dynamical (IV-B) and adapted specifically for hysteresis (IV-C) contexts. Numerical and experimental results are discussed in Sec. V. Finally, concluding remarks are given in Sec. VI.

II. BACKGROUND

A NARX (Nonlinear Autoregressive model with eXogenous inputs) polynomial model \mathcal{M} for a single-input single-output system is given by [25]:

$$y(k) = f^\ell(y(k-1), \dots, y(k-n_y), u(k-\tau_d), \dots, u(k-n_u)) + e(k), \quad (1)$$

where $u(k), y(k) \in \mathbb{R}$ are respectively the input and output signals sampled at instant $k \in \mathbb{N}$, and $f^\ell(\cdot)$ is a nonlinear polynomial function with degree $\ell \in \mathbb{N}^+$. $n_u, n_y \in \mathbb{N}^+$ are the maximum lags for u and y , respectively, $\tau_d \in \mathbb{N}^+$ is the pure time delay, and $e(k)$ accounts for the uncertainties and possible noise.

Model (1) is a parsimonious polynomial model in the sense that it contains only a small group of regressors chosen from an usually large set of candidate regressors by means of some structure selection procedure [22]–[24], [29], [30]. Each

regressor of \mathcal{M} , which can be any linear and nonlinear combination up to degree ℓ , is multiplied by a constant parameter, indicated by θ_i . Hence, a NARX polynomial model is linear-in-the-parameters and classic least squares (LS) procedures can be used [31]. In the presence of noise, however, it is common to add moving average (MA) terms to the model, which will no longer be linear-in-the-parameters. Fortunately, extended least squares estimators (ELS) can be used to circumvent noise-induced bias [22], [32].

A. Steady-state analysis

The steady-state relation of model (1) is obtained by taking $u(k) = \bar{u}$ and $y(k) = \bar{y}$, $\forall k$, thus yielding:

$$\bar{\mathcal{M}} : \bar{y} = \bar{f}^\ell(\bar{u}, \bar{y}),$$

which, for a known value of \bar{u} , can be rewritten as:

$$c_{y, \ell_y}(\bar{u})\bar{y}^{\ell_y} + c_{y, \ell_y-1}(\bar{u})\bar{y}^{\ell_y-1} + \dots + c_{y,1}(\bar{u})\bar{y} + c_{y,0}(\bar{u}) = 0, \quad (2)$$

where $1 \leq \ell_y \leq \ell$ is the degree of the static model $\bar{\mathcal{M}}$, whose coefficients $c_{y,i}$, $i = 0, \dots, \ell_y$ usually depend on \bar{u} . Solving (2) for the unknown \bar{y} is achieved by finding the ℓ_y roots of this polynomial. The roots of (2) will yield the fixed points of model (1) for \bar{u} , whose definition is presented below.

Definition 1. (Fixed points [33]). *The steady-state analysis of model (1) is computed by taking $y(k) = \bar{y}$, $\forall k$ and $u(k) = \bar{u}$, $\forall k$, yielding $\bar{y} = \bar{f}^\ell(\bar{y}, \bar{u})$, whose solution/root(s) \bar{y} (2) for a given constant value of input \bar{u} is defined as the fixed point(s), or equilibria, of model (1) for \bar{u} .*

The condition for (local) stability of the fixed points is obtained by finding the eigenvalues of the Jacobian matrix of model \mathcal{M} (1) evaluated at each fixed point, as follows:

$$\left| \text{eig} \left(\frac{\partial f^\ell}{\partial \mathbf{y}} \Big|_{\bar{\mathbf{y}}, \bar{\mathbf{u}}} \right) \right| < 1, \quad (3)$$

where $\mathbf{y} = [y(k-1) \dots y(k-n_y)]^T$, T is the transpose and $\text{eig}(\cdot)$ indicates the eigenvalues.

Example 1. Consider model \mathcal{M} given by:

$$y(k) = \hat{\theta}_1 y(k-1) + \hat{\theta}_2 u(k-1) + \hat{\theta}_3 u(k-1)u(k-2) + \hat{\theta}_4 u(k-1)^2 + \hat{\theta}_5 u(k-1)^3, \quad (4)$$

for which $\tau_d=1$, $n_y=1$, $n_u=2$, and $\ell=3$. Its static form $\bar{\mathcal{M}}$ is obtained taking $u(k-1)=u(k-2)=\bar{u}$ and $y(k-1)=y(k)=\bar{y}$, such that:

$$\bar{y} = \hat{\theta}_1 \bar{y} + \hat{\theta}_2 \bar{u} + \hat{\theta}_3 \bar{u}^2 + \hat{\theta}_4 \bar{u}^2 + \hat{\theta}_5 \bar{u}^3, \quad (5)$$

which can be written in the format of (2) as:

$$0 = \underbrace{[\hat{\theta}_1 - 1]}_{c_{y,1}} \bar{y} + \underbrace{[\hat{\theta}_3 + \hat{\theta}_4] \bar{u}^2 + \hat{\theta}_2 \bar{u}}_{c_{y,0}(\bar{u})}. \quad (6)$$

Hence, model (4) only has one fixed point for each value of \bar{u} , given by:

$$\bar{y} = -\frac{c_{y,0}(\bar{u})}{c_{y,1}} = \frac{\hat{\theta}_5 \bar{u}^3 + [\hat{\theta}_3 + \hat{\theta}_4] \bar{u}^2 + \hat{\theta}_2 \bar{u}}{1 - \hat{\theta}_1}. \quad (7)$$

For the first-order model (4), the Jacobian “matrix” will be a scalar and condition (3) becomes:

$$\begin{aligned} \left| \frac{\partial f^\ell}{\partial y(k-1)} \Big|_{\bar{u}, \bar{y}} \right| &< 1, \\ \left| \hat{\theta}_1 \Big|_{\bar{u}, \bar{y}} \right| &< 1, \\ -1 &< \hat{\theta}_1 < 1. \end{aligned} \quad (8)$$

Therefore, if (8) is satisfied, then (7) is a stable fixed point. \square

III. STATEMENT OF THE PROBLEM

It is assumed that a NARX model \mathcal{M} (1) is available for a given nonlinear dynamical system \mathcal{S} , estimated from input-output data $Z^N = \{u(k), y_s(k)\}_{k=1}^N$ collected from \mathcal{S} . Based on \mathcal{M} , the aim is to design a compensator \mathcal{M}_r such that the open-loop combination of \mathcal{M}_r followed by \mathcal{S} (see Fig. 1) is more linear and therefore more amenable for control. Specifically, \mathcal{M}_r should compensate the nonlinearity in \mathcal{S} .

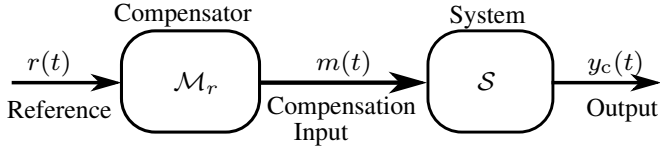


Fig. 1. Block diagram of the compensated system.

Mathematically, we require that the reference $r(k)$ and output $y_c(k)$ of the compensated system should be closer than the input $u(k)$ and output $y_s(k)$ of the uncompensated system. Hence $J[r(k), y_c(k)] < J[u(k), y_s(k)]$, where J is some proximity cost function, like the mean squared value.

IV. METHODOLOGY

This section presents the methodology developed to design compensators based on NARX polynomial models. First, in Sec. IV-A, we present the static compensation that is simpler to understand and serves as a basis for the main result, which is the dynamical compensation detailed in Sec. IV-B. In the sequel, this approach is applied to systems with hysteresis in Sec. IV-C. The identification of model \mathcal{M} is not described in this paper. The interested reader is referred to [27], and references therein.

A. Static Compensation

It is assumed that the input and output signals are bounded, thus $u(k) \in [u_{\min}, u_{\max}]$, $\forall k$ and $y_s(k) \in [y_{\min}, y_{\max}]$, $\forall k$. As for model $\mathcal{M}(1)$, the following assumptions will be needed:

Assumption 1. \mathcal{M} is valid, that is, $y(k) \approx y_s(k)$ for the same input.

Assumption 2. For any $\bar{u} \in [u_{\min}, u_{\max}]$, the model \mathcal{M} has at least one local stable fixed point such that $\bar{y} \in [y_{\min}, y_{\max}]$.

In order to obtain a static compensator $\bar{\mathcal{M}}_r$, an *inverse problem* in steady-state has to be solved. In other words, we

seek the system input values \bar{m} that will drive the output to the reference at steady-state, $\bar{y} \approx \bar{r}$. Considering the model \mathcal{M} expressed as $\bar{y} = \bar{f}^\ell(\bar{u}, \bar{y})$, \bar{y} is replaced by \bar{r} and \bar{u} by \bar{m} so that $\bar{\mathcal{M}}_r$ is $\bar{r} = \bar{f}^\ell(\bar{m}, \bar{r})$. Consequently, it is possible to rewrite (2) by grouping its terms in such a way that it yields a polynomial in the unknown variable \bar{m} , $\bar{\mathcal{M}}_r$:

$$c_{m, \ell_m}(\bar{r})\bar{m}^{\ell_m} + c_{m, \ell_m-1}(\bar{r})\bar{m}^{\ell_m-1} + \dots + c_{m, 1}(\bar{r})\bar{m} + c_{m, 0}(\bar{r}) = 0. \quad (9)$$

Although each of the ℓ_m roots of (9) is a solution to the inverse problem, not all are appropriate to be used in practice. For this reason, two constraints are considered. The used root:

Constraint C1) *must be real*, $m \in \mathbb{R}$; and

Constraint C2) *must be within the data range*, namely $m \in [u_{\min}, u_{\max}]$.

Assumption 2 ensures that any root \bar{m} (9) that satisfies the above constraints will drive the system to a stable fixed point. Also, because of Assumption 1, such a steady-state will satisfy $\bar{y}_c \approx \bar{r}$. The algebraic procedure is illustrated below with a simple example. Then, in the sequel, a dynamical version of this procedure will be discussed in Sec. IV-B.

Example 2. For the model in Example 1, it was seen that:

$$\bar{y} = \hat{\theta}_1 \bar{y} + \hat{\theta}_2 \bar{u} + \hat{\theta}_3 \bar{u}^2 + \hat{\theta}_4 \bar{u}^2 + \hat{\theta}_5 \bar{u}^3,$$

which can be written in the format of (9) as:

$$\begin{aligned} \bar{r} &= \hat{\theta}_1 \bar{r} + \hat{\theta}_2 \bar{m} + \hat{\theta}_3 \bar{m}^2 + \hat{\theta}_4 \bar{m}^2 + \hat{\theta}_5 \bar{m}^3, \\ 0 &= \underbrace{\hat{\theta}_5}_{c_{m,3}} \bar{m}^3 + \underbrace{[\hat{\theta}_3 + \hat{\theta}_4]}_{c_{m,2}} \bar{m}^2 + \underbrace{\hat{\theta}_2}_{c_{m,1}} \bar{m} + \underbrace{[\hat{\theta}_1 \bar{r} - \bar{r}]}_{c_{m,0}(\bar{r})}. \end{aligned} \quad (10)$$

Hence, for a given reference value \bar{r} , the roots of (10) provide potential compensation inputs that in steady-state would drive the system to the target. A practical problem is to decide which of the three roots in this example should be used. If there is only one real root, then it is chosen as the compensation input. However, if there are three real roots, a more general decision-making process is required. \square

For the sake of clarity, the roots of (9) will be placed in a vector $\bar{\mathbf{m}}(\bar{r}) \triangleq [\bar{m}_1 \dots \bar{m}_{\ell_m}]^T$. Although the ℓ_m values of \bar{m} are solutions to the inverse problem, only those that satisfy C1 and C2 should be considered as potential compensation inputs. This reasoning underlies the main algorithm that will be used in the dynamical context. The practical issue of *how* to choose from two potential inputs that satisfy C1 and C2 will be discussed in the dynamical setting below.

B. Dynamical Compensation

The main difference between the framework developed in this subsection and the basis laid down in the previous one is that here the reference is a sequence of values $r(k)$, and not a constant value \bar{r} . The same is true for the compensation input $m(k)$ and the compensated output $y_c(k)$.

The aim now is to achieve $y(k) \approx r(k)$ by solving an inverse problem dynamically. Replacing variables as in Sec. IV-A and omitting the noise term, (1) can be written as:

$$r(k) = f^\ell(r(k-1), \dots, r(k-n_y), m(k-\tau_d), \dots, m(k-n_u)).$$

As will become clear, it is convenient to introduce the time-shift $k \leftarrow k + \tau_d$ – meaning that k will be replaced with $k + \tau_d$ – hence the last equation becomes:

$$r(k + \tau_d) = f^\ell(r(k + \tau_d - 1), \dots, r(k + \tau_d - n_y), m(k), \dots, m(k + \tau_d - n_u)). \quad (11)$$

The aim is to find $m(k)$ that will drive the system to the desired target $r(k)$. Consequently, as before, (11) will be expressed in terms of a polynomial in the unknown $m(k)$ as:

$$0 = c_{\ell_m}(k)m(k)^{\ell_m} + c_{\ell_m-1}(k)m(k)^{\ell_m-1} + \dots + c_1(k)m(k) + c_0(k), \quad (12)$$

where the time-varying coefficients $c_j(k)$, $j = 0, \dots, \ell_m$, can depend on past values of m up to time $k - 1$, and on past and future values of r up to time $k + \tau_d$. Hence, the following additional assumption is required in the dynamical case.

Assumption 3. The reference signal must be known up to time $k + \tau_d$.

The following example illustrates this procedure.

Example 3. Consider the same model used in Example 1, replacing $y(k)$ with $r(k)$ and $u(k)$ with $m(k)$, yields:

$$r(k) = \hat{\theta}_1 r(k-1) + \hat{\theta}_2 m(k-1) + \hat{\theta}_3 m(k-1)m(k-2) + \hat{\theta}_4 m(k-1)^2 + \hat{\theta}_5 m(k-1)^3,$$

for which $\tau_d = 1$. Next, taking the time-shift $k \leftarrow k + 1$, the last equation can be expressed in the form of (12):

$$\begin{aligned} 0 &= \hat{\theta}_5 m(k)^3 + \hat{\theta}_4 m(k)^2 + [\hat{\theta}_2 + \hat{\theta}_3 m(k-1)]m(k) \\ &\quad + [\hat{\theta}_1 r(k) - r(k+1)], \\ 0 &= c_3(k)m(k)^3 + c_2(k)m(k)^2 + c_1(k)m(k) + c_0(k), \end{aligned} \quad (13)$$

where all the values of r are known (see Assumption 3) and also all past values of m . Hence, at each time step k the solutions to (13), that is, the three values of $m(k)$ are the potential compensation inputs. \square

In what follows, some important recommendations on initialization and the decision-making process adopted to choose the root to be used as compensation input are stated.

Remark 1. (Initial compensator conditions). From Assumption 3, $r(k + \tau_d)$ is known in compensator (12). Call that value \bar{r} . Using the calibration curve of \mathcal{S} or the static nonlinearity of \mathcal{M} , find the respective \bar{m} and take $m(j) = \bar{m}$, $j = k - 1, \dots, k + \tau_d - n_u$. If the calibration curve is not available, this value can be obtained through the static nonlinearity of model \mathcal{M} or by solving the static compensator \mathcal{M}_r (9), $\bar{r} = \bar{f}^\ell(\bar{m}, \bar{r})$, for \bar{m} . If there is more than one solution to $\bar{r} = \bar{f}^\ell(\bar{m}, \bar{r})$ use the one that: i) stabilizes the model output and ii) satisfies constraints C1 and C2. Items i) and ii) are automatically taken into account by using the calibration curve or static nonlinearity. \square

Remark 2. (The decision-making process). Let $\mathbf{m}_k \triangleq [m_1^k \dots m_{\ell_m}^k]^T$ be the set of roots of (12). If only one element of \mathbf{m}_k satisfies C1 and C2, then this will be the compensation

input at time k , otherwise we choose the appropriate root according to:

$$m(k) = \arg \min_{m_j^k, \forall j \in \{1, \dots, \ell_m\}} (|m_j^k - m(k-1)|). \quad (14)$$

subject to: C1, C2

The use of (14) selects the solution that is closest to the compensation value used in the previous time step. This simple criterion results in smoother signals $m(k)$ and, consequently, in less compensation effort [21]. \square

If ℓ_m is even and composed only of complex conjugate values, then take $m(k) = m(k-1)$. This situation is not common for models that satisfy Assumption 1. Algorithm 1 summarizes the method to select the appropriate root.

Algorithm 1: Selecting the Appropriate Solution for (12)

Input: $m(k-1)$; $\mathbf{m}_k \triangleq [m_1^k \dots m_{\ell_m}^k]^T$
 $v \leftarrow \infty$
 $a \leftarrow 0$
for $j = 1$ **to** ℓ_m **do**
 if $m_j^k \in \mathbb{R}$ (C1) **and** $u_{\min} \leq m_j^k \leq u_{\max}$ (C2) **then**
 $e \leftarrow |m_j^k - m(k-1)|$
 if $e < v$ **then**
 $v \leftarrow e$
 $a \leftarrow 1$
 $m(k) \leftarrow m_j^k$
 end
 end
end
if $a = 0$ **then**
 $m(k) \leftarrow m(k-1)$
end
Output: $m(k)$

C. Compensation for Systems with Hysteresis

The inclusion of the first difference of the input $u(k)$ and the corresponding sign function as regressors is a sufficient condition for NARX models to mimic hysteresis loop [26]. A general NARX model set [34] extended with these regressors will be referred to as \mathcal{M}_h :

$$y(k) = g^\ell(y(k-1), \dots, y(k-n_y), u(k-\tau_d), \dots, u(k-n_u), \phi_1(k-1), \phi_2(k-1)) + e(k), \quad (15)$$

where $\phi_1(k) = u(k) - u(k-1)$, $\phi_2(k) = \text{sign}(\phi_1(k))$, $g^\ell(\cdot)$ is a polynomial function of the regressor variables up to degree ℓ , and the other parameters are the same as defined in (1). For models such as (15), there are two sets of equilibria for the deterministic part (omitting the noise) under loading-unloading inputs: one for loading with $\phi_2(k) = 1$, and one for unloading with $\phi_2(k) = -1$ [21]. A constrained approach is proposed and detailed by [21] to ensure that the model can describe the dynamic behaviour and also features in steady-state.

Therefore, to deal specifically with hysteresis compensation, the general compensation method proposed in Sec. IV-B will

be adapted. Considering non-constant inputs, the following simplification will be used:

$$\begin{aligned}\phi_1(k-1)\phi_2(k-1) &= \phi_1(k-1)\frac{|\phi_1(k-1)|}{\phi_1(k-1)}, \\ &= |u(k-1) - u(k-2)|, \quad (16)\end{aligned}$$

for $u(k-1) \neq u(k-2)$.

The compensator is developed following the *steps* below:

1) Rewrite \mathcal{M}_h as:

$$0 = g^\ell(y(k-1), \dots, y(k-n_y), u(k-\tau_d), \dots, u(k-n_u), \phi_1(k-1), \phi_2(k-1)) - y(k); \quad (17)$$

- 2) if $\phi_1(k-1)\phi_2(k-1)$ appears in any regressor of (17), use the result in (16);
- 3) if $\phi_1(k-1)$ and $\phi_2(k-1)$ still appear, replace them with $u(k-1) - u(k-2)$ and $|u(k-1) - u(k-2)|/[u(k-1) - u(k-2)]$, respectively;
- 4) if $[u(k-1) - u(k-2)]$ appears in any denominator, multiply the equation by $[u(k-1) - u(k-2)]$;
- 5) replace $y(k)$ with $r(k)$, $u(k)$ with $m(k)$, perform the time shift $k \leftarrow k + \tau_d$, and rewrite this equation like (12);
- 6) split the equation with $|\cdot|$ into two polynomials in $m(k)$:

$$\begin{aligned}0 &= c_{\ell_m}^L(k)m(k)^{\ell_m} + c_{\ell_m-1}^L(k)m(k)^{\ell_m-1} \\ &+ \dots + c_1^L(k)m(k) + c_0^L(k) \quad (18) \\ &\text{for } m(k) > m(k-1),\end{aligned}$$

$$\begin{aligned}0 &= c_{\ell_m}^U(k)m(k)^{\ell_m} + c_{\ell_m-1}^U(k)m(k)^{\ell_m-1} \\ &+ \dots + c_1^U(k)m(k) + c_0^U(k) \quad (19) \\ &\text{for } m(k) < m(k-1),\end{aligned}$$

where the superscripts L and U refer to loading and unloading regimes, respectively. Note that, as we are now dealing with a hysteretic system, (12) has two counterparts: one for loading (18), and one for unloading (19). In this case, the compensation input $m(k)$ will be a feasible root of (18) or (19). Before detailing the decision-making process to compensate for such systems, the previous steps will be illustrated below.

Example 4. Suppose that the model \mathcal{M}_h is:

$$\begin{aligned}y(k) &= \hat{\theta}_1 y(k-1) + \hat{\theta}_2 u(k-1)^3 + \hat{\theta}_3 \phi_1(k-1)\phi_2(k-1)u(k-1) \\ &+ \hat{\theta}_4 \phi_1(k-1)\phi_2(k-1)y(k-1).\end{aligned} \quad (20)$$

Following steps 1 and 2, (20) is rewritten as:

$$\begin{aligned}0 &= \hat{\theta}_1 y(k-1) + \hat{\theta}_2 u(k-1)^3 + \hat{\theta}_3 |u(k-1) - u(k-2)|u(k-1) \\ &+ \hat{\theta}_4 |u(k-1) - u(k-2)|y(k-1) - y(k).\end{aligned} \quad (21)$$

In this model, steps 3 and 4 do not apply. By means of step 5, we get the following equation (remember that $\tau_d = 1$):

$$\begin{aligned}0 &= \hat{\theta}_1 r(k) + \hat{\theta}_2 m(k)^3 + \hat{\theta}_3 |m(k) - m(k-1)|m(k) \\ &+ \hat{\theta}_4 |m(k) - m(k-1)|r(k) - r(k+1), \quad (22)\end{aligned}$$

which can be split into two polynomials (step 6) as:

$$\begin{aligned}0 &= \hat{\theta}_2 m(k)^3 + \hat{\theta}_3 m(k)^2 + \\ &[-\hat{\theta}_3 m(k-1) + \hat{\theta}_4 r(k)]m(k) + \\ &[\hat{\theta}_1 r(k) - \hat{\theta}_4 m(k-1)r(k) - r(k+1)] \\ &\text{for } m(k) > m(k-1), \quad (23)\end{aligned}$$

$$\begin{aligned}0 &= \hat{\theta}_2 m(k)^3 - \hat{\theta}_3 m(k)^2 + \\ &[\hat{\theta}_3 m(k-1) - \hat{\theta}_4 r(k)]m(k) + \\ &[\hat{\theta}_1 r(k) + \hat{\theta}_4 m(k-1)r(k) - r(k+1)] \\ &\text{for } m(k) < m(k-1).\end{aligned} \quad (24)$$

Here, (23) refers to loading regime similar to form (18) with $c_3^L(k) = \hat{\theta}_2$, $c_2^L(k) = \hat{\theta}_3$, $c_1^L(k) = -\hat{\theta}_3 m(k-1) + \hat{\theta}_4 r(k)$, and $c_0^L(k) = \hat{\theta}_1 r(k) - \hat{\theta}_4 m(k-1)r(k) - r(k+1)$; while, in an analogous way, (24) refers to unloading regime in form (19) with coefficients $c_3^U(k) = \hat{\theta}_2$, $c_2^U(k) = -\hat{\theta}_3$, $c_1^U(k) = \hat{\theta}_3 m(k-1) - \hat{\theta}_4 r(k)$, and $c_0^U(k) = \hat{\theta}_1 r(k) + \hat{\theta}_4 m(k-1)r(k) - r(k+1)$.

The polynomials (23) and (24), which are valid for $k \geq 1$, can be initialized, at $k = 0$, using an estimate of the hysteresis loop, as will be illustrated in Example 5. \square

In addition to Assumption 3, C1 and C2, the following must also be true for hysteretic systems:

Constraint C3 $m(k) > m(k-1)$, if (18) is used at time k ;
OR

Constraint C4 $m(k) < m(k-1)$, if (19) is used at time k .

Constraints C3 and C4 are needed to ensure that the root is consistent with the regime for which it was calculated. Therefore, the decision-making process for hysteretic systems is similar to that explained in Remark 2 with the addition of these new constraints. Hence:

$$m(k) = \arg \min_{m_j^k, \forall j \in \{1, \dots, \ell_m\}} (|m_j^k - m(k-1)|), \quad (25)$$

subject to: C1, C2, Cq

where $q \in \{3, 4\}$. The step-by-step procedure is analogous to Algorithm 1, but now using (25) instead of (14).

D. Initialization of Compensators for Systems with Hysteresis

If any parameter of compensators (18) and (19) depends on previous values of the compensation input $m(k)$, i.e. $\{m(k-1), \dots, m(k+\tau_d-n_u)\}$, such values must be determined for initialization. In Sec. IV-B, we can use the static curve to estimate these initial values, as described in Remark 1. Here, a hysteresis loop \mathcal{H} behavior displayed on the input-output plane will be used. In what follows, a procedure is described to obtain \mathcal{H} for a given model \mathcal{M}_h (15).

Consider the following sinusoidal input signal with period $T = 1/f_{\min}$:

$$\tilde{u}(k) = A \sin(2\pi f_{\min} k) + \tilde{u}_0, \quad (26)$$

where $f_{\min} = 1/T$ is the lowest frequency of interest, $\tilde{u}_0 = (u_{\min} + u_{\max})/2$ is the mean, and $A = u_{\max} - \tilde{u}_0$ is the amplitude. Using $\tilde{u}(k)$ in the model (15), after the transient, the resulting data set $\{\tilde{u}(k), \tilde{y}(k)\}_{k=N_i}^{N_e}$, where $N_i > T$ and $N_e = N_i + T$, correspond to a hysteresis loop \mathcal{H} . The use

of \mathcal{H} to initialize the compensator is illustrated in the next example.

Example 5. Consider model (20) of Example 4, whose parameter values are $\hat{\theta}_1 = 0.8$, $\hat{\theta}_2 = 0.4$, $\hat{\theta}_3 = 0.2$, and $\hat{\theta}_4 = 0.1$. In order to initialize the compensator, at $k = 0$, $m(-1)$ is needed in (23) and (24). For this purpose, suppose that the excitation input signal \tilde{u} (26) is defined with $A = 1$, $f_{\min} = 1$ Hz, and $\tilde{u}_0 = 1$ for which the resulting \mathcal{H} is shown in Fig. 2.

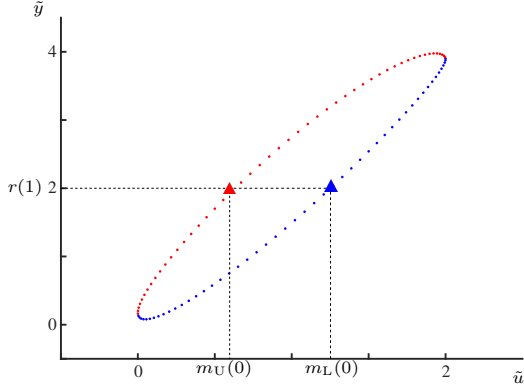


Fig. 2. Loop \mathcal{H} is obtained from the simulation of model (20) with the input described in Example 5. Blue dots (\bullet) refer to loading regime, while those in red (\bullet) refer to unloading. For a given output or reference, say $r(1)$, there are two possible inputs indicated by triangles (\blacktriangle) blue and red (\blacktriangle) that correspond to $m_L(0)$ and $m_U(0)$, respectively. Which of these to use to start computing the compensator is determined by the regime at initialization time.

From Assumption 3, we have that the reference is known up to time $r(k+1)$. Suppose that $r(1) = 2$ and that $\tilde{y} = r(1)$, there are two possible values for the input \tilde{u} , namely of, $m_L(0)$ and $m_U(0)$, which can be obtained from \mathcal{H} (Fig. 2). The selection between these values is made based on the current regime of the reference signal, i.e., loading ($r(1) - r(0) > 0$) or unloading ($r(1) - r(0) < 0$). In this example, at $k = 0$, the reference is in the loading regime and, therefore, $m(0) = m_L(0)$ is chosen to initialize equations (23) and (24). \square

V. RESULTS

This section illustrates the compensator design proposed in Sec. IV for two simulated benchmark systems and for a pilot plant starting from the identified models. The input design and other identification procedures are detailed in [35]. To evaluate the performance of the compensation achieved, the static nonlinearity of the compensated and uncompensated systems are compared and their time evolution is evaluated using the mean absolute percentage error (MAPE) index is computed as follows:

$$\text{MAPE} = \frac{\sum_{k=1}^N |y_s(k) - y(k)|}{N |\max(\mathbf{y}_s) - \min(\mathbf{y}_s)|}. \quad (27)$$

A. A Heating System

The bench test system is a small electrical heater modeled by the following Hammerstein model [36]:

$$\begin{aligned} y(k) &= \beta_1 y(k-1) + \beta_2 v(k-1) + \beta_3 y(k-2) + \beta_4 v(k-2), \\ v(k) &= p_1 u(k)^2 + p_2 u(k), \end{aligned} \quad (28)$$

where $y(k)$ is the normalized temperature, and $u(k)$ is the electric power applied to the heater within the range $0 \leq u(k) \leq 1$. The data set has been presented in [13], and is available at <https://bit.ly/3iQ6rCF>. The operation region of the model is $u(k) \in [0, 1]$ and $y(k) \in [0, 0.5]$. As described in [35], the obtained parameters of (28) are: $p_1 = 4.639331 \times 10^{-1}$, $p_2 = 5.435865 \times 10^{-2}$; while $\beta_1 = 1.205445$, $\beta_2 = 8.985133 \times 10^{-2}$, $\beta_3 = -3.0877507 \times 10^{-1}$ and $\beta_4 = 9.462358 \times 10^{-3}$. From now on, the Hammerstein model (28) will be treated as the system \mathcal{S} to be compensated.

To compensate the nonlinearities in \mathcal{S} , the following three-term model \mathcal{M} was obtained according to the procedure detailed in [35]:

$$y(k) = \hat{\theta}_1 y(k-1) + \hat{\theta}_2 u(k-2)^2 + \hat{\theta}_3 y(k-2), \quad (29)$$

where $\hat{\theta}_1 = 8.958185 \times 10^{-1}$, $\hat{\theta}_2 = 6.393347 \times 10^{-2}$, and $\hat{\theta}_3 = -1.746750 \times 10^{-2}$. The validation results are shown in Table I, which indicate some degradation at higher frequencies and at points of operation close to the origin.

TABLE I
MAPE FOR MODEL (29) WITH SINUSOIDAL INPUTS
 $u(k) = u_0 + 0.2\sin(2\pi fk)$. FREE-RUN SIMULATION WAS USED.

f [Hz]	u_0 [V]		
	0.3	0.5	0.7
0.0005	5.5%	3.0%	2.9%
0.001	5.8%	2.9%	2.8%
0.002	7.0%	4.0%	3.1%

The static function of \mathcal{M} (29) is:

$$\bar{y} = \frac{\hat{\theta}_2 \bar{u}^2}{1 - \hat{\theta}_1 - \hat{\theta}_3}, \quad (30)$$

from where it is seen that for each value of the input, there is only one fixed point. Because \mathcal{M} is second-order, there are two eigenvalues at each fixed point \bar{y} . The Jacobian matrix in this case does not depend on \bar{u} or \bar{y} . Using (3) the condition for stability is:

$$\left| \text{eig} \left(\begin{bmatrix} 0 & 1 \\ \hat{\theta}_3 & \hat{\theta}_1 \end{bmatrix} \right) \right| < 1,$$

where the eigenvalues of the Jacobian matrix are the algebraic solutions of $\lambda^2 - \hat{\theta}_1 \lambda - \hat{\theta}_3 = 0$, which yields $|\lambda_1| = 0.8759$ and $|\lambda_2| = 0.0199$. Therefore, the fixed point for each input value is stable and, consequently, Assumption 2 is satisfied.

To illustrate the static compensation method presented in Sec. IV-A, \bar{y} is replaced with \bar{r} and \bar{u} with \bar{m} in (30) to find a polynomial in the unknown \bar{m} , that can be expressed like (9):

$$\begin{aligned} \bar{r} &= \frac{\hat{\theta}_2 \bar{m}^2}{1 - \hat{\theta}_1 - \hat{\theta}_3}, \\ 0 &= \underbrace{[\hat{\theta}_2]}_{c_{m,2}} \bar{m}^2 + \underbrace{[(\hat{\theta}_1 + \hat{\theta}_3 - 1)\bar{r}]}_{c_{m,0}(\bar{r})}. \end{aligned} \quad (31)$$

Since (31) is an incomplete quadratic equation and the operation region is limited to $0 \leq \bar{m} \leq 1$, the algebraic solution is given by:

$$\bar{m} = \sqrt{\frac{-c_{m,0}(\bar{r})}{c_{m,2}}} = \sqrt{\frac{(1 - \hat{\theta}_1 - \hat{\theta}_3)\bar{r}}{\hat{\theta}_2}}. \quad (32)$$

Also, as $\bar{r} \geq 0$, $\hat{\theta}_2 > 0$ and $1 - \hat{\theta}_1 - \hat{\theta}_3 > 0$, the result of the square root in (32) is always real. In Fig. 3, the static compensation results are shown for a reference that is a sequence of steps. As expected, the compensated system is approximately linear (see Fig. 3-b). The static compensation can be used to find the initial values for the dynamical compensator when needed.

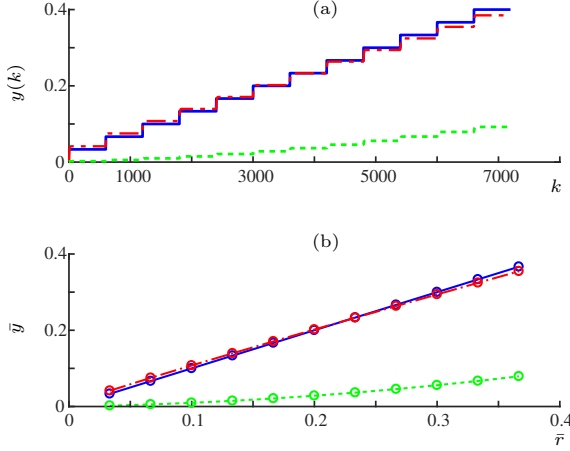


Fig. 3. Validation results for static compensation: (—) is the reference; (---), output of the compensated system; (· · ·), output of the uncompensated system. In (a), temporal evolution of the outputs and the reference; (b), the $r \times y$ plane.

For dynamical compensation, using model \mathcal{M} (29) the procedure put forward in Sec. IV-B yields (see Eq. 11):

$$r(k+1) = \hat{\theta}_1 r(k) + \hat{\theta}_2 m(k)^2 + \hat{\theta}_3 r(k-1)$$

and (see Eq. 12):

$$0 = \underbrace{[\hat{\theta}_2]}_{c_2} m(k)^2 + \underbrace{[\hat{\theta}_1 r(k) + \hat{\theta}_3 r(k-1) - r(k+1)]}_{c_0(k)}. \quad (33)$$

Solving (33) at each iteration yields the compensation input $m(k)$. Because (33) is quadratic, there are two possibilities. Either both roots are real, and then Algorithm 1 is used to select which one to use, or the roots are complex conjugate in which case the previous value is used, i.e., $m(k) = m(k-1)$.

The algebraic solution of (33) gives the compensator \mathcal{M}_r :

$$m(k) = \sqrt{\frac{-c_0(k)}{c_2}} = \sqrt{\frac{r(k+1) - \hat{\theta}_1 r(k) - \hat{\theta}_3 r(k-1)}{\hat{\theta}_2}}. \quad (34)$$

Because $m(k)$ does not depend on its previous values, in order to initialize (34), it is sufficient to make $r(-1) = r(0)$ in (34) at $k = 0$.

In Fig. 4 and in Table II, the results obtained with \mathcal{M}_r (34) is compared to the uncompensated system for different reference signals. The uncompensated results are performed using $r(k)$ as the input for \mathcal{S} . From Table II, it is seen that as the frequency increases, the compensation becomes somewhat less effective, as would be expected for most control systems. Also for small values of $r(k)$ (see Fig. 4-b), complex roots appear, and according to Algorithm 1, the last computed value will be used, that is, $m(k) = m(k-1)$.

Figure 5 shows the results for a Monte Carlo test of 10000 runs. During each run, a perturbed model \mathcal{M} (29) is obtained

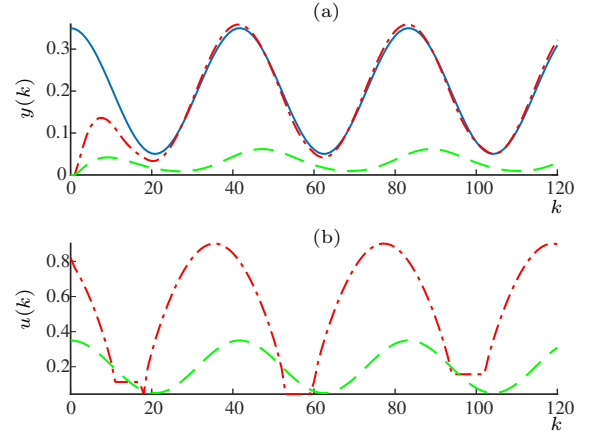


Fig. 4. Compensation results. (a) temporal evolution; (b) the applied inputs. In (a), (—) is the reference $r(k) = 0.2\sin(2\pi(0.002)k + \pi/2) + 0.15$; (---) is the output of the compensated system $y_c(k)$ and (· · ·) is the output of the system $y_s(k)$ without compensation. In (b), (---) is the compensation input $m(k)$, while (· · ·) is the input applied in the uncompensated system.

TABLE II
MAPE FOR COMPENSATED AND UNCOMPENSATED SYSTEMS WITH
 $r(k) = r_0 \sin(2\pi f k + \pi/2) + r_0$.

	f [Hz]	0.05	r_0 [V]	0.10	0.20
Compensated	0.0005	7.8%	4.1%	3.4%	
	0.001	9.4%	6.4%	5.6%	
	0.002	15.5%	12.2%	10.2%	
	0.004	29.5%	25.8%	20.2%	
Uncompensated	0.0005	45.6%	44.0%	40.8%	
	0.001	45.5%	44.0%	40.9%	
	0.002	45.3%	44.0%	41.4%	
	0.004	44.8%	43.7%	41.8%	

by taking parameters from a Gaussian distribution centered at the original parameters and with the covariance matrix of the estimator. The black dashed lines indicate the region determined by $\mu(\bar{r}) \pm 2\sigma(\bar{r})$, where $\mu(\bar{r})$ is the output mean and $\sigma(\bar{r})$ is the standard deviation. The compensation performance is considerably effective on average for $\bar{r} < 0.3$, and then it degrades a bit.

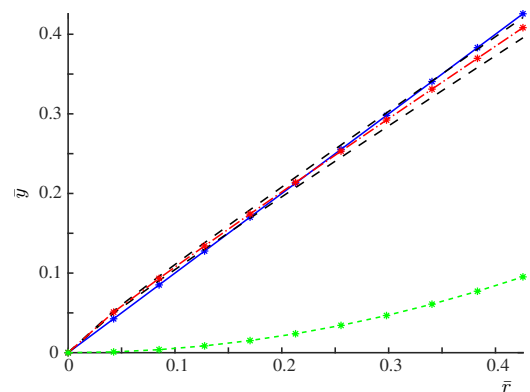


Fig. 5. Results of a Monte Carlo test. (· · ·) static curve of the uncompensated system, (---) is the reference and (---) is $\mu(\bar{r})$, the mean calculated for the 10000 runs at each value \bar{r} , (· · ·) represent the error bars of $\pm 2\sigma(\bar{r})$.

B. A Hysteretic System

In this example, the following Bouc-Wen model was used to describe the hysteretic behavior of a piezoelectric actuator

(PZT) that is an unimorph cantilever [5]:

$$\begin{aligned} \dot{h}(t) &= \alpha_{\text{bw}}\dot{u}(t) - \beta_{\text{bw}}|\dot{u}(t)|h(t) - \gamma_{\text{bw}}\dot{u}(t)|h(t)|, \\ y(t) &= \nu_y u(t) - h(t), \end{aligned} \quad (35)$$

where $u(t)$ [V] is the voltage input, $y(t)$ [μm] is the position output, the parameters $\alpha_{\text{bw}} = 0.9[\mu\text{m}/\text{V}]$ and $\beta_{\text{bw}} = \gamma_{\text{bw}} = 0.008[\text{V}^{-1}]$ determine the hysteresis loop, while $\nu_y = 1.6[\mu\text{m}/\text{V}]$ is a weight factor for the output. Here, (35) is referred as the system \mathcal{S} to be compensated, which is simulated with a fourth-order Runge-Kutta method considering the integration step $\delta_t = 5\text{ms}$.

The following NARX polynomial model \mathcal{M}_h (15) to represent \mathcal{S} was obtained as detailed in [35]:

$$\begin{aligned} y(k) &= \hat{\theta}_1 y(k-1) + \hat{\theta}_2 \phi_2(k-1) \phi_3(k-1) u(k-1) \\ &\quad + \hat{\theta}_3 \phi_2(k-1) \phi_3(k-1) y(k-1) + \hat{\theta}_4 \phi_2(k-1), \end{aligned} \quad (36)$$

where $\hat{\theta}_1 = 1.000099$, $\hat{\theta}_2 = 6.630567 \times 10^{-3}$, $\hat{\theta}_3 = -6.247018 \times 10^{-3}$, and $\hat{\theta}_4 = 7.892915$. The validation results are shown in Table III, which indicate some degradation at higher frequencies and amplitudes.

TABLE III

MAPE FOR MODEL (36) WITH SINUSOIDAL INPUTS $u(k) = G\sin(2\pi fk)$. FREE-RUN SIMULATION WAS USED.

f [Hz]	G [V]		
	10	30	50
0.2	2.6%	2.0%	4.7%
1.0	2.7%	1.3%	4.1%
5.0	7.7%	5.0%	3.6%

Following steps 1, 2, 3 and 5 for the procedure presented in Sec. IV-C, the compensator obtained is $\mathcal{M}_{h,r}$ given by:

$$\begin{aligned} 0 &= \hat{\theta}_1 r(k) - r(k+1) + \hat{\theta}_2 |m(k) - m(k-1)| m(k) \\ &\quad + \hat{\theta}_3 |m(k) - m(k-1)| r(k) + \hat{\theta}_4 |m(k) - m(k-1)|, \end{aligned} \quad (37)$$

for which is assumed that $m(k) \neq m(k-1)$, and it can be split into two polynomials in $m(k)$, like (18) and (19) in step 6, as:

$$0 = c_2^L m(k)^2 + c_1^L(k) m(k) + c_0^L(k), \quad \text{for } m(k) > m(k-1); \quad (38)$$

and

$$0 = c_2^U m(k)^2 + c_1^U(k) m(k) + c_0^U(k), \quad \text{for } m(k) < m(k-1), \quad (39)$$

where $c_2^L = \hat{\theta}_2$, $c_1^L(k) = -\hat{\theta}_2 m(k-1) + \hat{\theta}_3 r(k) + \hat{\theta}_4$, $c_0^L(k) = \hat{\theta}_1 r(k) - \hat{\theta}_3 m(k-1) r(k) - \hat{\theta}_4 m(k-1) - r(k+1)$, $c_2^U = -\hat{\theta}_2$, $c_1^U(k) = \hat{\theta}_2 m(k-1) - \hat{\theta}_3 r(k) - \hat{\theta}_4$, and $c_0^U(k) = \hat{\theta}_1 r(k) + \hat{\theta}_3 m(k-1) r(k) + \hat{\theta}_4 m(k-1) - r(k+1)$.

As some parameters of (38) and (39) depend on $m(k-1)$, the initialization of the compensator is required at $k = 0$. Applying $\tilde{u} = 50\sin(2\pi 0.2k)$ to model \mathcal{M}_h (36), the loop $\mathcal{H}(\tilde{u}, \tilde{y})$ is determined. Making $\tilde{y} = r(k+1)$, $m(k-1)$ can be determined directly from loop \mathcal{H} similarly to Example 5.

The validation results for compensation with (38) and (39) are shown in Fig. 6 and in Table IV. These results indicate that the compensated system presents better tracking performance than the uncompensated in all evaluated scenarios. In addition, the worst results occur at higher frequencies and amplitudes.

Finally, Fig. 7 shows the results for 10000 Monte Carlo runs, where $r(k) = 20\sin(2\pi(2)k + \pi/2)$ is used in 5 cycles. A

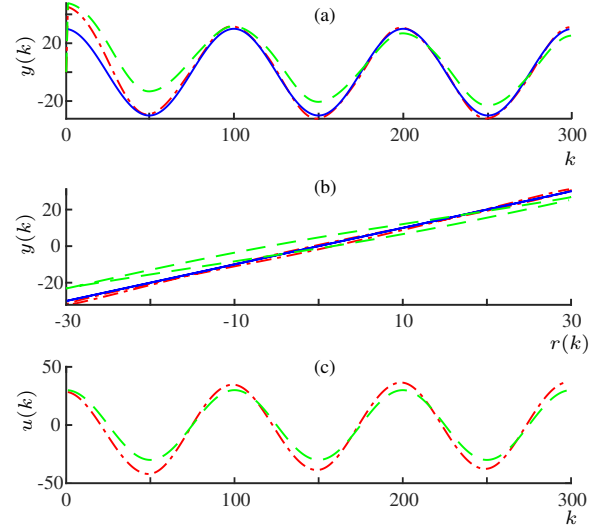


Fig. 6. Compensation results for system (35). (a) temporal evolution of outputs; (b) the $r \times y$ plane and (c) temporal evolution of inputs. (-) represents the reference $r(k) = 30\sin(2\pi(2)k + \pi/2)$; (-*-), results for compensator given by (38) and (39) and (- -), uncompensated system.

TABLE IV

MAPE FOR COMPENSATED AND UNCOMPENSATED SYSTEMS WITH $r(k) = G_0\sin(2\pi fk + \pi/2)$.

	f [Hz]	G_0 [μm]		
		20	30	40
Compensated	0.2	1.4%	3.2%	5.2%
	1.0	0.9%	2.5%	4.5%
	2.0	1.0%	1.4%	3.4%
	5.0	5.4%	4.5%	3.9%
Uncompensated	0.2	7.8%	7.1%	6.4%
	1.0	7.8%	7.0%	6.3%
	2.0	7.7%	6.9%	6.1%
	5.0	7.6%	6.6%	5.8%

perturbed model \mathcal{M}_h (36) is obtained, as before. The Monte Carlo test presents a region determined by $\mu(k) \pm 2\sigma(k)$, where $\mu(k)$ and $\sigma(k)$ are analogous to those described in Sec. V-A, now for each k , instead of \bar{r} . Comparing with Fig. 5, the error bars determine a wider region. It is explained due to the sensitivity of \mathcal{M}_h on variations in $\hat{\theta}_2$.

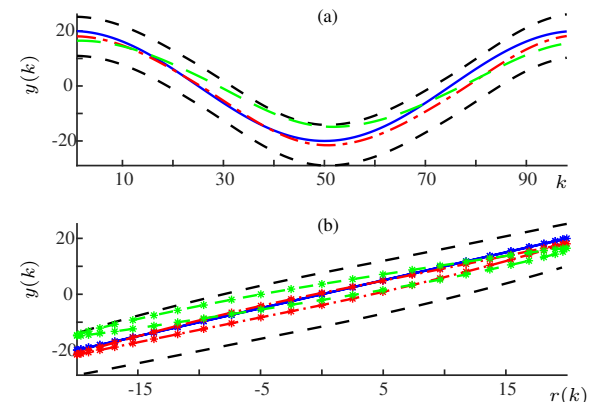


Fig. 7. Results for 10000 Monte Carlo runs. (a) temporal evolution of the outputs in the last cycle; (b) plane $r(k) \times y(k)$. (-*-) refers to the uncompensated system, (-*-*) refers to the reference and (-*-*) is the average $\mu(k)$ of the 10000 Monte Carlo runs for the compensated system. (- -) represent the error bars of $\pm 2\sigma(k)$.

It should be mentioned that the constraint $\Sigma_y = 1$ presented by [21] is not fulfilled, where $\Sigma_y = 1$ is the sum of all linear output's regressors. In order to show how this constraint affects the behavior of the model and compensator, we use a constrained least squares estimator to impose $\Sigma_y = 1$ on the parameters of (36). The model obtained with constraints, $\mathcal{M}_{h,\text{cns}}$, has the same structure of \mathcal{M}_h (36) with parameters: $\Sigma_y = \hat{\theta}_{1,\text{cns}} = 1$, $\hat{\theta}_{2,\text{cns}} = 6.630913 \times 10^{-3}$, $\hat{\theta}_{3,\text{cns}} = -6.157515 \times 10^{-3}$, and $\hat{\rho}_{4,\text{cns}} = 7.893146$.

Because the equal framework of \mathcal{M}_h and $\mathcal{M}_{h,\text{cns}}$, their compensators also have a same polynomial structure. The compensator $\mathcal{M}_{h,\text{cns},r}$ is obtained when we replace each corresponding parameter of $\mathcal{M}_{h,\text{cns}}$ in (38) and (39). Since the results obtained for modeling and compensation are similar to those presented by Tables III and IV, these results are omitted.

A more relevant comparison for these two models and compensators is shown in Fig. 8. In this figure, the performance of the models and compensators is verified when an input/reference sinusoidal signal becomes constant. Note that the validation and compensation results for \mathcal{M}_h (36) do not converge at steady-state. As $\bar{\phi}_1 = \bar{\phi}_2 = 0$, both models become $\bar{y} = \Sigma_y \bar{y}$ that have a single eigenvalue equal to Σ_y . Consequently, as $\Sigma_y = \hat{\theta}_1 > 1$, \mathcal{M}_h is unstable in steady-state while the constraint $\Sigma_y = \hat{\theta}_{1,\text{cns}} = 1$, makes $\mathcal{M}_{h,\text{cns}}$ remains in the last state. The compensation methods work in an open-loop, hence steady-state errors are expected, but they tend to be less significant for more precise models. For the current example, it was found that model \mathcal{M}_h has a steady-state error that tends to infinity over time, while the constrained model $\mathcal{M}_{h,\text{cns}}$ provides a steady-state error of approximately $0,26\mu\text{m}$ in Fig. 8-(b). Such errors are reflected in the compensation performance since $\mathcal{M}_{h,\text{cns},r}$ presents an offset error of $0.83\mu\text{m}$ in Fig. 8-(d) while the other, $\mathcal{M}_{h,r}$, has a steady-state error which tends to infinity similarly to its model.

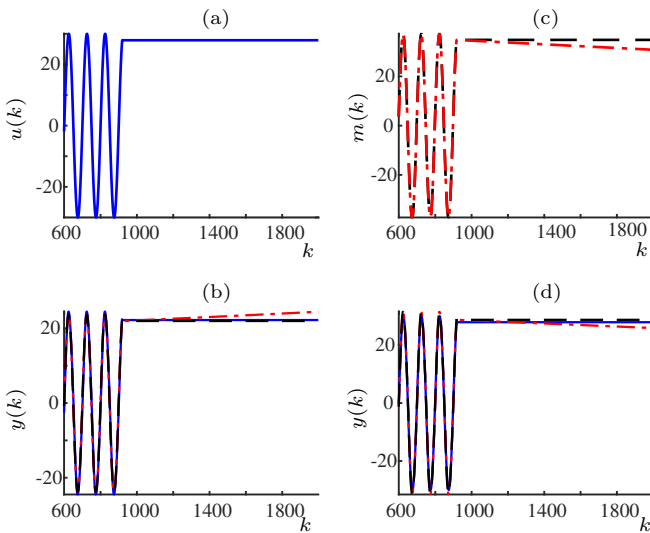


Fig. 8. Validation and compensation results for models \mathcal{M}_h and $\mathcal{M}_{h,\text{cns}}$ when a sinusoidal input or reference become constant. In (a), we have the temporal evolution of the input $u(k) = 30\sin(2\pi(2)k)$ that becomes constant at $k = 920$. This input determines the outputs in (b) when applied to the system \mathcal{S} (—), to \mathcal{M}_h (---) and to $\mathcal{M}_{h,\text{cns}}$ (- -). In (c), $m(k)$ for \mathcal{M}_h (---) and $\mathcal{M}_{h,\text{cns}}$ (- -) that were calculated for $r(k) = u(30\sin(2\pi(2)k))$. Finally, (d) shows the respective outputs for (c) where $r(k)$ is (—).

C. Experimental Results

In this section, the compensation strategy is applied to an experimental pneumatic control valve, which is a type of actuator widely used in industrial processes. For this type of actuator, the control performance can degrade significantly due to friction, dead-zone, dead-band, and hysteresis [38], [39].

The present valve is the same used in [21], where the measured output is its stem position and the input is a pressure signal applied to the valve after passing V/I and I/P conversion. The sampling time is $T_s = 0.01\text{ s}$ and, for details of the identification of this system the reader is referred to [21], [35]. The following models will be considered in this case study.

1) \mathcal{M}_h is the model identified with the inclusion of $\phi_1(k)$ and $\phi_2(k)$ as candidate regressors [26], and with the gray-box restrictions proposed by [21]. As shown in Fig. 8, the use of such constraints is important to describe the behavior in steady-state. The estimated model is

$$\begin{aligned} y(k) &= \hat{\theta}_1 y(k-1) + \hat{\theta}_2 y(k-2) + \hat{\theta}_3 \phi_1(k-1) \\ &+ \hat{\theta}_4 u(k-1) \phi_1(k-1) \phi_2(k-1) \\ &+ \hat{\theta}_5 y(k-2) \phi_1(k-1) \phi_2(k-1), \end{aligned} \quad (40)$$

with $\hat{\theta}_1 = 9.76 \times 10^{-1}$, $\hat{\theta}_2 = 2.40 \times 10^{-2}$, $\hat{\theta}_3 = 1.19 \times 10^{-1}$, $\hat{\theta}_4 = 3.76$ and $\hat{\theta}_5 = -4.73$. Note that, $\Sigma_y = \hat{\theta}_1 + \hat{\theta}_2 = 1$.

The following models are found in the literature.

2) \mathcal{M}_{bw} is used to represent a BW model (35). To estimate the valve output, its parameters were re-estimated using an evolutionary approach based on niches, which is formulated in [40]. These parameters are: $\alpha_{\text{bw}} = 7.54 \times 10^{-1}$, $\alpha_{\text{bw}} = -4.96$, $\gamma_{\text{bw}} = -3.61$ and $\nu_y = 7.54 \times 10^{-1}$.

The last two models adopted were identified in [21] for the same system under study and with the same identification data.

3) $\mathcal{M}_{h,2}$ was identified – see Eq. 33 in [21] – with the same constraints used for \mathcal{M}_h (40), plus an additional one such that the input signal can be isolated when writing the compensator equation.

4) $\check{\mathcal{M}}_h$ was identified to describe the inverse relationship between $u(k)$ and $y(k)$ of the valve – see Eq. 34 in [21]. Therefore, the model provides $\hat{u}(k)$ given $y(k)$. The set of candidate regressors includes $\check{\phi}_1(k) = y(k) - y(k-1)$ and $\check{\phi}_2(k) = \text{sign}[\check{\phi}_1(k)]$.

The performance of the direct models, the first three, subject to sinusoidal inputs with different amplitudes are shown in Table V, which indicate that these models have similar efficiency by MAPE. Since $\check{\mathcal{M}}_h$ is an inverse model, which predicts the input signal instead of the output and must be simulated from a smoothed version of $y(k)$ [21], we do not directly compare the MAPE accuracy of this model with the others. More details can be found in [35].

For each model, the respective compensator is shown below. The first compensator is obtained following the strategy presented in Sec. IV-C.

1) The compensator for \mathcal{M}_h (40) is $\mathcal{M}_{h,r}$, obtained with the application of steps 1, 2, 3, 5 and 6. $\mathcal{M}_{h,r}$ is compound by two quadratic polynomials like (38) and (39) with parameters: $c_2^L = \hat{\theta}_4$, $c_1^L(k) = \hat{\theta}_3 - \hat{\theta}_4 m(k-1) + \hat{\theta}_5 r(k-1)$, $c_0^L(k) =$

TABLE V
MAPE FOR MODELS VALIDATION WITH SINUSOIDAL INPUTS
 $u(t) = G_0 \sin(2\pi(0.1)t + \pi/4) + 3V$.

Model	G_0 [V]			
	0.45	0.55	0.65	0.75
1 - \mathcal{M}_h	3.6%	3.0%	3.1%	4.9%
2 - \mathcal{M}_{bw}	3.9%	4.1%	4.5%	6.5%
3 - $\mathcal{M}_{h,2}$	3.2%	3.5%	3.9%	5.7%

$$\hat{\theta}_1 r(k) + \hat{\theta}_2 r(k-1) + \hat{\theta}_3 m(k-1) - \hat{\theta}_5 r(k-1)m(k-1) - r(k+1),$$

$$c_2^U = -\hat{\theta}_4, c_1^T(k) = -\hat{\theta}_3 + \hat{\theta}_4 m(k-1) - \hat{\theta}_5 r(k-1) \text{ and } c_0^L(k) = \hat{\theta}_1 r(k) + \hat{\theta}_2 r(k-1) - \hat{\theta}_3 m(k-1) + \hat{\theta}_5 r(k-1)m(k-1) - r(k+1).$$

2) The compensation law $m(t)$, for model \mathcal{M}_{bw} , was proposed by [5], and is referred as $\mathcal{M}_{bw,r}$ given by:

$$m(t) = \frac{10}{7.21} [r(t) + h(t)]. \quad (41)$$

3) The compensator for $\mathcal{M}_{h,2}$ namely $\mathcal{M}_{h,2,r}$ is given by Eq. 35 in [21].

4) Finally, also extracted from [21], $\check{\mathcal{M}}_{h,r}$, the compensator for $\check{\mathcal{M}}_h$ is given by Eq. 36 in the mentioned paper.

The compensation results for sinusoidal references with different amplitudes are shown in Table VI while Fig. 9 shows the compensation results for one of these references, $r(k) = 0.41 \sin(2\pi(0.1)t + \pi/4) + 3V$. All compensation strategies provide considerably better results in all evaluated scenarios when compared to the uncompensated system.

TABLE VI
MAPE FOR COMPENSATED AND UNCOMPENSATED SYSTEMS WITH
 $r(t) = G_0 \sin(2\pi(0.1)t) + 3.07V$.

Compensation Strategy	G_0 [V]			
	0.26	0.34	0.41	0.50
1) $\mathcal{M}_{h,r}$ (38-39)	3.9%	3.3%	3.3%	3.8%
2) $\mathcal{M}_{bw,r}$ (41)	5.9%	4.4%	4.3%	4.2%
3) $\mathcal{M}_{h,2,r}$ (35) in [21]	3.6%	3.5%	3.9%	5.2%
4) $\check{\mathcal{M}}_{h,r}$ (36) in [21]	2.9%	2.8%	3.2%	2.7%
Uncompensated	21.0%	18.0%	16.2%	14.4%

For the uncompensated system, the input is the reference $r(k)$. Using this as a starting point, we would like to quantify how much more has to be done in order to achieve compensation. To this end, the following is computed

$$E(\delta_m) = \sum_{k=N-N_0}^{N-1} \delta_m(k)^2, \quad (42)$$

where $\delta_m(k) = |m(k) - r(k)|$ and N is the length of $\delta_m(k)$. $E(\delta_m)$ can be interpreted as the energy of $\delta_m(k)$ over one period N_0 . Also, the variability with respect to the uncompensated system is given by the standard deviation of $\delta_m(k)$, $\sigma(\delta_m)$, see Table VII for a summary of results.

Similar to the validation results of model \mathcal{M}_{bw} , the corresponding compensator $\mathcal{M}_{bw,r}$ (41) performs slightly worse compared to those based on NARX models. This suggests that NARX models are more appropriated to describe nonlinearities in the valve. This is not surprising, as the class of NARX polynomials is more general than the Bouc-Wen class. On the positive side, the Bouc-Wen model provided the

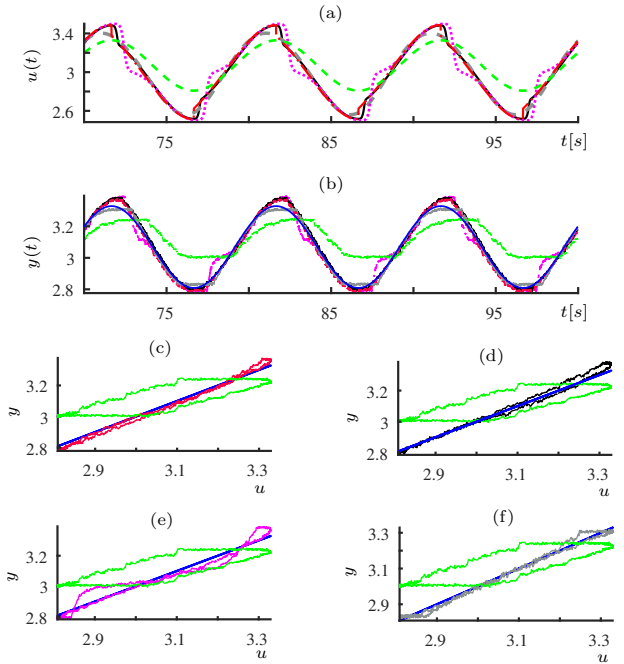


Fig. 9. Compensation results for the pneumatic valve. (a) temporal evolution of compensation inputs in three cycles; (b) temporal evolution of outputs for the compensated systems in three cycles; (c)-(f) show the $r \times y$ plane for each compensator. (—) refers to the reference $r(t) = 0.34 \sin(2\pi(0.1)t + \pi/4) + 3V$; (—), uncompensated system; (---) compensation with $\mathcal{M}_{h,r}$ (38-39); (—) compensation with $\mathcal{M}_{bw,r}$ (41); (· · ·) compensation with $\mathcal{M}_{h,2,r}$ (35) in [21]; (—) compensation with $\mathcal{M}_{h,r}$ (36) in [21].

TABLE VII
 $E(\delta_m)[\sigma(\delta_m)]$ FOR THE INVESTIGATED COMPENSATORS WITH
 $r(t) = G_0 \sin(2\pi(0.1)t) + 3.07V$.

Strategy	G_0 [V]			
	0.26	0.34	0.41	0.50
1) $\mathcal{M}_{h,r}$ (38-39)	28.3 [0.154]	33.7 [0.165]	39.4 [0.174]	49.4 [0.186]
2) $\mathcal{M}_{bw,r}$ (41)	27.0 [0.149]	33.3 [0.163]	40.6 [0.178]	53.7 [0.197]
3) $\mathcal{M}_{h,2,r}$ (35) in [21]	38.7 [0.184]	43.7 [0.193]	50.1 [0.203]	57.2 [0.206]
4) $\check{\mathcal{M}}_{h,r}$ (36) in [21]	24.9 [0.139]	38.3 [0.174]	52.7 [0.203]	72.6 [0.237]

simplest compensator among those presented. In addition, as seen in Table VII the respective compensator requires little change compared to the uncompensated system. The most challenging task related to the Bouc-Wen model is to estimate its parameters, which was done with an evolutionary approach.

Both compensation strategies proposed by [21] performed well. $\mathcal{M}_{h,2,r}$ requires special care in the phase of structure selection otherwise the compensation input $m(k)$ cannot be computed explicitly. Apart from that the compensation law tends to be easier to calculate than the one put forward in this work. On the negative side, $\mathcal{M}_{h,2,r}$ produces inputs with more abrupt changes (see Fig. 9-(a) and (e)). This is reflected in higher values of $E(\delta_m)$ and $\sigma(\delta_m)$.

The overall good performance of compensator $\check{\mathcal{M}}_{h,r}$ comes at the expense of careful data preprocessing [21]. This compensator can produce smooth compensation inputs (Fig. 9-(a) and (f)) with low MAPE values (Table VI). However $E(\delta_m)$ and $\sigma(\delta_m)$ tend to increase considerably with the reference amplitude, as shown in Table VII.

The compensator designed with the methodology put forward in this work, $\mathcal{M}_{h,r}$, was also able to compensate for the nonlinearity in the valve. The MAPE are among the lowest,

especially for moderate-high reference amplitudes, G_0 , with the advantage that $E(\delta_m)$ and $\sigma(\delta_m)$ do not increase as much as for the other regulators with G_0 (Table VII). In addition, \mathcal{M}_h has only 5 terms which facilitates obtaining the compensation law. Also, if the parameters of such model needed to be updated, a recursive algorithm can be readily implemented. On the other hand, if the process models turn out to be polynomials with degree greater than 3, numerical solvers would be required to find the roots. Fortunately, many systems can be adequately described using polynomials up to third-degree. As a side note, there is a self-consistency check indirectly provided by the current method, which is the appearance of unfeasible roots: either real but outside the operating range or complex. Whenever this happens it is an indication that the process model is not adequate. Fortunately no such problems occurred in this case study.

VI. CONCLUSION

This work has presented an approach to compensate nonlinearities based on NARX polynomial models previously estimated. The method is simple and easy to interpret, as the compensation input turns out to be the value required for the system to attain steady-state properties. The compensation input is obtained iteratively, which confers some adaptability to the method. The degree of adaptability can be readily increased by estimating the model parameters recursively, this has not been explored in the paper.

The method has been considered in three contexts: static for constant references, dynamical for variant, and for systems with hysteresis. At first, the technique was illustrated using two simulated systems. The performance is comparable to that of other methods available in the literature. In addition, the method presents some robustness to variation in the parameters, as evaluated using Monte Carlo tests.

The proposed technique was also implemented on a pilot plant where the goal was to compensate the nonlinearity of a pneumatic control valve. The performance was compared with a compensator designed in [5] and two more recent strategies published by [21]. All compensators can achieve nonlinearity compensation for the valve (see Table VI). Pros and cons of each technique were discussed.

Another interesting feature of the presented technique is that a compensator can be designed for linear or nonlinear systems with or without using constraints during model estimation. Perhaps the main foreseen limitation occurs if the compensators are designed using polynomial models of degree greater than 3, which is not a common situation in practice, though it could happen. In this case, it would be necessary to use numerical solvers to find the roots, which could turn out to be a problem for more demanding online applications. Fortunately, many relevant systems can be described by models up to 3rd degree for which the roots can be found with analytical expressions presented in Appendix A.

Finally, the aim of the compensators is to cancel out most of the nonlinearity. This would allow for the design of linear feedback controllers as a second step.

APPENDIX A

SOLVING ALGEBRAIC POLYNOMIAL EQUATIONS

Algebraic polynomial equations with unknown x , degree $n \in \mathbb{N}^+$, and known coefficients $a_i \in \mathbb{R}$, $i \in \{0, \dots, n\}$, can be expressed as

$$0 = a_n x^n + a_{n-1} x^{n-1} + \dots + a_1 x + a_0, \quad a_n \neq 0 \quad (43)$$

For (43), there are n complex roots. The analytical solutions for $n \leq 3$ are presented in the sequel.

A) Linear Equations

$$0 = a_1 x + a_0, \quad a_1 \neq 0$$

$$x = \frac{-a_0}{a_1}$$

B) Quadratic Equations

$$0 = a_2 x^2 + a_1 x + a_0, \quad a_2 \neq 0$$

$$\Delta = a_1^2 - 4a_2 a_0$$

$$x_i = \frac{-a_1 + (-1)^i \Delta}{2a_2}, \quad i \in \{0, 1\}$$

C) Cubic Equations

$$0 = a_3 x^3 + a_2 x^2 + a_1 x + a_0, \quad a_3 \neq 0$$

$$\Delta_0 = a_2^2 - 3a_3 a_1$$

$$\Delta_1 = 2a_2^3 - 9a_3 a_2 a_1 + 27a_3^2 a_0$$

$$C = \sqrt[3]{\frac{\Delta_1 \pm \sqrt{\Delta_1^2 - 4\Delta_0^3}}{2}}$$

$$\xi = \frac{-1 + \sqrt{-3}}{2}$$

$$x_i = -\frac{1}{3a} \left(b + \xi^i C + \frac{\Delta_0}{C} \right), \quad i \in \{0, 1, 2\}$$

ACKNOWLEDGMENT

PEOGBA and LAA gratefully acknowledge financial support from CNPq (Grant Nos. 142194/2017-4 and 303412/2019-4) and FAPEMIG (TEC-1217/98).

REFERENCES

- [1] R. Isermann and M. Münchhof, *Identification of dynamic systems: an introduction with applications*. Springer Science & Business Media, 2010.
- [2] S. A. Billings, *Nonlinear system identification: NARMAX methods in the time, frequency, and spatio-temporal domains*. John Wiley & Sons, 2013.
- [3] O. Nelles, *Nonlinear system identification: from classical approaches to neural networks and fuzzy models*. Springer Science & Business Media, 2013.
- [4] J. Schoukens and L. Ljung, "Nonlinear system identification: A user-oriented road map," *IEEE Control Systems Magazine*, vol. 39, no. 6, pp. 28–99, 2019.
- [5] M. Rakotondrabe, "Bouc-Wen Modeling and Inverse Multiplicative Structure to Compensate Hysteresis Nonlinearity in Piezoelectric Actuators," *IEEE Transactions on Automation Science and Engineering*, vol. 8, no. 2, pp. 428–431, 2011.
- [6] J. Li and H. Tian, "Position control of SMA actuator based on inverse empirical model and SMC-RBF compensation," *Mechanical Systems and Signal Processing*, vol. 108, pp. 203–215, 2018.
- [7] H. Cao, Y. Zhang, C. Shen, Y. Liu, and X. Wang, "Temperature energy influence compensation for MEMS vibration gyroscope based on RBF NN-GA-KF method," *Shock and Vibration*, vol. 2018, 2018.

- [8] T. Hong, A. J. Morris, M. N. Karim, J. Zhang, and W. Luo, "Nonlinear control of a wastewater pH neutralisation process using adaptive narx models," in *1996 IEEE International Conference on Systems, Man and Cybernetics. Information Intelligence and Systems (Cat. No.96CH35929)*, vol. 2, 1996, pp. 911–916 vol.2.
- [9] B. Singh, V. Verma, and J. Solanki, "Neural network-based selective compensation of current quality problems in distribution system," *IEEE Transactions on Industrial Electronics*, vol. 54, no. 1, pp. 53–60, 2007.
- [10] F. L. Chernous'ko, I. M. Ananievski, and S. A. Reshmin, *Control of nonlinear dynamical systems: methods and applications*. Springer Science & Business Media, 2008.
- [11] K. A. Morris, "What is hysteresis?" *Applied Mechanics Reviews*, vol. 64, p. 050801, 2012.
- [12] O. Castillo and P. Melin, *Soft computing for control of non-linear dynamical systems*. Physica, 2012, vol. 63.
- [13] L. A. Aguirre, M. Corrêa, and C. C. S. Cassini, "Nonlinearities in NARX polynomial models: representation and estimation," *Proc. IEE Part D: Control Theory and Applications*, vol. 149, no. 4, pp. 343–348, 2002.
- [14] C. Lin, H. Yau, and Y. Tian, "Identification and Compensation of Nonlinear Friction Characteristics and Precision Control for a Linear Motor Stage," *IEEE/ASME Transactions on Mechatronics*, vol. 18, no. 4, pp. 1385–1396, 2013.
- [15] L. Liu, L. Li, Y. Huang, K. Cui, Q. Xiong, F. N. Hauske, C. Xie, and Y. Cai, "Intrachannel nonlinearity compensation by inverse volterra series transfer function," *Journal of Lightwave Technology*, vol. 30, no. 3, pp. 310–316, 2011.
- [16] G. Quaranta, W. Lacarbonara, and S. F. Masri, "A review on computational intelligence for identification of nonlinear dynamical systems," *Nonlinear Dynamics*, 2020.
- [17] Y. Zhou, A. Wang, P. Zhou, H. Wang, and T. Chai, "Dynamic performance enhancement for nonlinear stochastic systems using RBF driven nonlinear compensation with extended Kalman filter," *Automatica*, vol. 112, p. 108693, 2020.
- [18] X. Zhang, Y. Tan, M. Su, and Y. Xie, "Neural networks based identification and compensation of rate-dependent hysteresis in piezoelectric actuators," *Physica B: Condensed Matter*, vol. 405, no. 12, pp. 2687–2693, 2010.
- [19] K. Guo, Y. Pan, and H. Yu, "Composite learning robot control with friction compensation: a neural network-based approach," *IEEE Transactions on Industrial Electronics*, vol. 66, no. 10, pp. 7841–7851, 2018.
- [20] D. Meng, P. Xia, K. Lang, E. C. Smith, and C. D. Rahn, "Neural network based hysteresis compensation of piezoelectric stack actuator driven active control of helicopter vibration," *Sensors and Actuators A: Physical*, vol. 302, p. 111809, 2020.
- [21] P. E. O. G. B. Abreu, L. A. Tavares, B. O. S. Teixeira, and L. A. Aguirre, "Identification and nonlinearity compensation of hysteresis using NARX models," *Nonlinear Dynamics*, vol. 102, no. 1, pp. 285–301, 2020.
- [22] S. A. Billings, S. Chen, and M. J. Korenberg, "Identification of MIMO nonlinear systems using a forward-regression orthogonal estimator," *Int. J. Control*, vol. 49, no. 6, pp. 2157–2189, 1989.
- [23] L. A. Aguirre and S. A. Billings, "Improved structure selection for nonlinear models based on term clustering," *Int. J. Control*, vol. 62, no. 3, pp. 569–587, 1995.
- [24] L. Piroddi and W. Spinelli, "An identification algorithm for polynomial NARX models based on simulation error minimization," *Int. J. Control*, vol. 76, no. 17, pp. 1767–1781, 2003.
- [25] I. J. Leontaritis and S. A. Billings, "Input-output parametric models for nonlinear systems part I: Deterministic nonlinear systems," *Int. J. Control*, vol. 41, no. 2, pp. 303–328, 1985.
- [26] S. A. M. Martins and L. A. Aguirre, "Sufficient Conditions for Rate-Independent Hysteresis in Autoregressive Identified Models," *Mechanical Systems and Signal Processing*, vol. 75, pp. 607–617, 2016.
- [27] L. A. Aguirre, "A Bird's Eye View of Nonlinear System Identification," *arXiv:1907.06803 [eess.SY]*, 2019.
- [28] W. Lacerda Junior, S. A. M. Martins, E. Nepomuceno, and M. Lacerda, "Control of Hysteretic Systems Through an Analytical Inverse Compensation based on a NARX model," *IEEE Access*, vol. PP, pp. 1–1, 07 2019.
- [29] A. Falsone, L. Piroddi, and M. Prandini, "A randomized algorithm for nonlinear model structure selection," *Automatica*, vol. 60, pp. 227–238, 2015.
- [30] P. F. L. Retes and L. A. Aguirre, "NARMAX model identification using a randomized approach," *Int. J. Modelling, Identification and Control*, 2019.
- [31] J. P. Norton, *An Introduction to Identification*. London: Academic Press, 1986.
- [32] L. Ljung, *System Identification: Theory for the User*. New Jersey: Prentice Hall, 1987.
- [33] L. A. Aguirre and E. M. A. M. Mendes, "Global Nonlinear Polynomial Models: Structure, Term Clusters and Fixed Points," *International Journal of Bifurcation and Chaos*, vol. 6, no. 2, pp. 279–294, 1996.
- [34] S. A. Billings and S. Chen, "Extended model set, global data and threshold model identification of severely nonlinear systems," *Int. J. Control*, vol. 50, no. 5, pp. 1897–1923, 1989.
- [35] L. A. Tavares, P. E. O. G. B. Abreu, and L. A. Aguirre, "Identification of NARX Models for Compensation Design," *arXiv:2011.10109 [eess.SY]*, 2020.
- [36] L. A. Aguirre, M. C. S. Coelho, and M. V. Corrêa, "On the interpretation and practice of dynamical differences between Hammerstein and Wiener models," *Proc. IEE Part D: Control Theory and Applications*, vol. 152, no. 4, pp. 349–356, 2005.
- [37] R. Srinivasan and R. Rengaswamy, "Stiction Compensation in Process Control Loops: A Framework for Integrating Stiction Measure and Compensation," *Industrial & Engineering Chemistry Research*, vol. 44, no. 24, pp. 9164–9174, 2005.
- [38] M. A. A. S. Choudhury, S. L. Shah, and N. F. Thornhill, *Diagnosis of Process Nonlinearities and Valve Stiction: Data Driven Approaches*. Springer, Berlin Heidelberg, 2008.
- [39] R. A. Romano and C. Garcia, "Valve friction and nonlinear process model closed-loop identification," *Journal of Process Control*, vol. 21, no. 4, pp. 667–677, 2011.
- [40] L. A. Tavares, P. E. O. G. B. Abreu, and L. A. Aguirre, "Estimação de Parâmetros de Modelos Bouc-Wen via Algoritmos Evolutivos para Compensação de Histerese," in *Anais do 14º Simpósio Brasileiro de Automação Inteligente*, 2019.